Undrained cylindrical cavity expansion/contraction in stiff clays using a two-surface plasticity model

Wei Cheng, Ren-Peng Chen, Jean-Michel Pereira, Yu-Jun Cui

Undrained cylindrical cavity expansion/contraction in stiff clays using a two-surface plasticity model

Wei Cheng[1], Ren-peng Chen[2,*], Jean-Michel Pereira[3], Yu-jun Cui[4]

[1]*Former Ph.D student, Department of Civil Engineering, Zhejiang University, Hangzhou 310058, China, wcheng@zju.edu.cn*

[2]*Professor, Department of Civil Engineering, Zhejiang University, Hangzhou 310058, China; College of Civil Engineering, Hunan University, Changsha 410082, China; chenrp@zju.edu.cn, chenrp@hnu.edu.cn* (Corresponding author)

[3]*Professor, Laboratoire Navier (UMR 8205), Ecole des Ponts ParisTech, Univ Gustave Eiffel, CNRS, IFSTTAR, F-77455 Marne-la-Vallée, France*

[4]*Professor, Laboratoire Navier (UMR 8205), Ecole des Ponts ParisTech, Univ Gustave Eiffel, CNRS, IFSTTAR, F-77455 Marne-la-Vallée, France*

Abstract

This paper presents a semi-analytical solution of undrained cylindrical cavity expansion/contraction problem using a two-surface plasticity model for natural stiff clays from the view point of poromechanics. The present solution reduces the classical boundary problem into a group of seven first-order ordinary differential equations via an auxiliary independent variable ξ under undrained conditions. It strictly follows the premise of constant soil mass. Meanwhile, the solution for the constant soil volume problem is used for comparison. It shows that constant soil mass assumption is of paramount importance in developing solutions under high stress condition, while constant soil volume induces non-negligible errors in effective stress and pore pressure distributions. Based on the premise of constant soil mass, extensive parametric studies on cavity expansion/contraction are undertaken to investigate the effects of the model key parameters on the stress components distribution, excess pore pressure distribution and cavity expansion curves. The present solution could be useful while dealing with geotechnical and petroleum engineering problems involving stiff clays or soft claystones. The application in Praclay Gallery excavation in natural Boom clay well demonstrates the validity of the present solution.

Keywords: stiff clays; cavity expansion/contraction; undrained condition; constant soil mass; elastoplasticity; poromechanics

1. Introduction

Cavity expansion theory has been widely applied to interpreting the results from some in situ tests such as cone penetration and pressuremeter tests, analyzing the stresses and deformations induced by wellbore drilling, gallery excavation, tunneling and pile installation. Over the past decades, various analytical and semi-analytical solutions [1-13] for cylindrical and spherical cavity expansions have been developed. With the increasing complexity of constitutive models, from elastic models, elastic perfectly plastic models to critical state models, the solutions are increasingly realistic. Among these models, original and modified Cam-clay models have gained large popularity in solving the cavity expansion and contraction problems for their capability of modelling strain hardening/softening behaviors of soils. Carter et al. [14] firstly investigated the cavity expansion problems with original Cam-clay model by means of finite element analysis. Collins and Yu [6] developed a general solution for large strain undrained cavity expansion using both original and modified Cam-clay models with and without zero initial radius assumption. Cao et al. [7], by following Collins and Yu's approach, developed a semi-analytical solution for undrained cavity using modified Cam-clay model. Mo and Yu [8], extended the original Cam-clay model to a unified state parameter model for clays and sands, then developed a novel solution for both cylindrical and spherical cavity problems. Russell and Khalili [29], using the similarity technique, investigated the cavity expansion problem in unsaturated soils by a unified bounding surface model to consider the influence of suction and moisture content. That study demonstrated there was no difficulty in solving cavity expansion problems using two-surface constitutive models. However, it should be noted that the initial stress state is assumed isotropic and the vertical stress is omitted in two stress invariants in that similarity approach [6]. Recently, Chen and Abousleiman [9-11] proposed novel semi-analytical solutions for both drained and undrained cylindrical cavity expansion/contraction problems. Their solutions removed the limitation on the initial condition of isotropic stress state and depicted a more general case of in situ situation by considering the vertical stress around the expanded/contracted cavity. Based on this versatile framework, Chen et al. [12] used the semi-analytical solution to analyze the three-dimensional strength and the anisotropic properties of soils by introducing Spatially Mobilized Plane (SMP) criterion in modified Cam-clay model. More recently, fabric and stress induced anisotropy has

also been accounted for using anisotropic elastoplastic models like S-CLAY1 [13] and Dafalias' anisotropic bounding surface model [14]. Although various types of solutions have been proposed, most of them basically treat soil as an original or modified Cam-clay material with an associated flow rule, providing quite low accuracy in modelling heavily over-consolidated clays. In particular, for highly plastic stiff clays or soft claystone, high clay contents, low void ratios, low permeability and high stress states (usually greater than 1 MPa) distinguish them from Cam-clay materials with the following basic hydro-mechanical behaviors:

(1) Highly nonlinear behaviors are typically observed on stiff clays at heavily over-consolidated states [16]. These pre-yielding nonlinear behaviors would have significant influence on the variations of pore pressure and displacements which are described by advanced constitutive modelling for stiff clays [16, 17, 18, 22].

(2) For highly plastic stiff clays, the yield surface is of a 'tear' shape rather than an 'elliptical' shape. An 'elliptical' shape would overestimate the failure stress on the 'dry side' but underestimate it on the 'wet side'. The yield surface shape variation would lead to misestimating the excess pore pressure under undrained conditions. On the other hand, the plastic flow direction should also be considered for the complex behavior of stiff clays.

(3) The pore fluid governs the distribution of excess pore pressure and stress components in expanding process. In relatively low stress states (e.g. 0.1 MPa~1 MPa) under undrained conditions, the volumetric strain due to loading remains almost constant. However, for stiff clays and soft claystone at great depth (e.g. 1MPa~100MPa), the pore water would induce a slight volumetric strain itself, which can significantly influence the excess pore pressure.

These three main differences make the existing analytical solutions [6-14] difficult to be used directly in analyzing tunneling and piezocone penetration tests in stiff clays under deep ground. On the other hand, although several two-surface plasticity (bounding/subloading surface) models have already been numerically applied into tunnel/gallery construction, e.g. the ground movement (settlement or uplift) induced by tunneling in stiff London clay[38-39] or Shanghai soft clay[37], the excess pore water pressure distribution in Boom clay[35], the characteristic of load transfer in shanghai clay during tunnel operating period[36], the corresponding novel analytical or semi-analytical solutions are still appealing. Based on the rigorous semi-analytical framework proposed by Chen and Abousleiman [9] and the premise of constant soil mass, the study extends

the solution with a two-surface plasticity model named ACC2 [16] to consider the mechanical behavior of natural stiff clays under high stress conditions. After a brief introduction of the basic formulas, the main features and parameters of the two-surface plasticity model, it is extended to undrained conditions by incorporating the mass conservation for the liquid phase in the pore space. By using the incremental stress-strain relationship, the undrained cavity expansion/contraction problem is formulated to solve a system of first-order ordinary differential equations with two different premises, namely constant soil volume and constant soil mass, respectively. A discussion between Constant Soil Volume (CSV) and Constant Soil Mass (CSM) assumptions is included to highlight that undrained condition corresponds to a situation with constant soil mass. Further parametric studies based on four key material parameters about stress paths, stress distribution and cavity expansion/contraction curves are conducted. Lastly, as a precise and convenient tool, the present semi-analytical solution is utilized to predict the pore pressure and stress distribution along the radial distance and the supporting pressure which is required to maintain the Gallery stability in the case of Praclay Gallery in underground research facility HADES-URF built at a depth of 223m in natural Boom clay.

2. Model description

This section gives a brief description of the two-surface plasticity model for stiff clays (e.g. natural Boom clay) named ACC2 [16]. The formulation of ACC2 model is based on the triaxial conditions with three principal stresses (namely, σ_r', σ_θ', σ_z' in a cylindrical coordinate system):

$$p' = \frac{1}{3}\left(\sigma_r' + \sigma_\theta' + \sigma_z'\right) \tag{1}$$

$$q = \sqrt{\frac{1}{2}\left(\left(\sigma_r' - \sigma_\theta'\right)^2 + \left(\sigma_r' - \sigma_z'\right)^2 + \left(\sigma_\theta' - \sigma_z'\right)^2\right)} \tag{2}$$

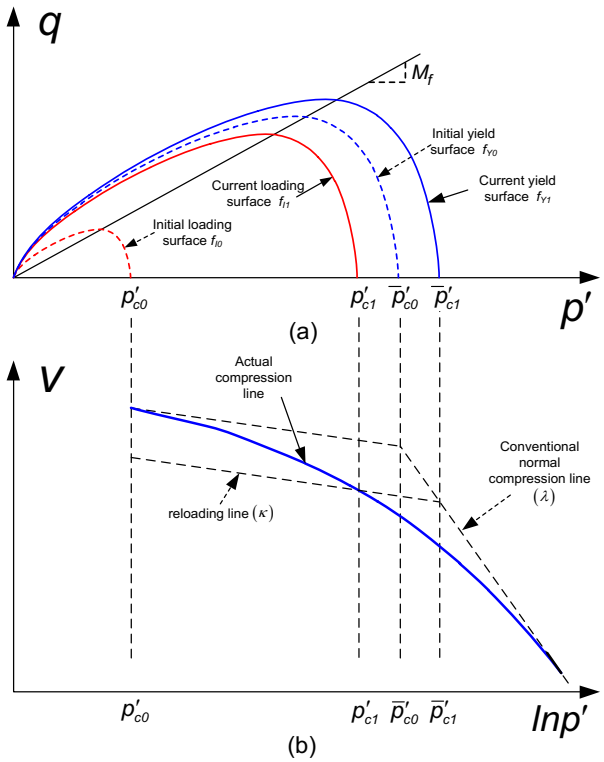

137

138 Fig.1 Schematic plot of two surface plasticity model ACC2: (a) p'-q plane; (b) v-ln p' plane

139 Fig.1 gives a schematic illustration of the two surfaces (Loading surface and Yield surface).
140 These two surfaces are linked through a progressive hardening relationship by a positive scalar r
141 in v-ln p' plane. A smooth compression behavior is achieved via the use of two hardening variables
142 $\bar{p}'_c$ and r before the soil reaches normally consolidated states:

143 $$r = \frac{p'}{\bar{p}'} = \frac{q}{\bar{q}} = \frac{p'_c}{\bar{p}'_c} \tag{3}$$

144 where p'_c is the actual loading yield stress on the Loading surface and $\bar{p}'_c$ is the conventional
145 pre-consolidation pressure on the conventional Normal Compression Line.

146 Similar to the concept of bounding surface plasticity, the current stress point (p', q) is
147 assumed to always lie on the Loading surface which is expressed as:

148 $$f_l\left(p', q, r, p'_c\right) = q^2 + \frac{M_f^2}{1-k_f}\left(\frac{p'}{r\bar{p}'_c}\right)^{\frac{2}{k_f}}\left(r\bar{p}'_c\right)^2 - \frac{M_f^2 p'^2}{1-k_f} = 0 \tag{4}$$

149 where M_f is the stress ratio at the apex of the two surfaces and k_f is a parameter specifying the
150 shape of the yield surfaces. Because natural stiff clays (e.g. natural Boom clay) show a unique
151 yielding behavior, a generalized yield surface ($k_f < 2$) is adopted in this model. While k_f varies

from 0.5 to 2, a tear shape surface turns into an elliptical shape more suitable to soft clays in Fig. 2(a). The calibrated yielding behavior of natural Boom clay shows that the closest value of k_f is 0.7.

Two internal variables, namely $\bar{p}_c'$ and r, are used to control the plastic strain hardening or softening behavior. A cam-clay type volumetric plastic strain isotropic hardening law for $d\bar{p}_c'$ is adopted:

$$d\bar{p}_c' = \frac{\upsilon}{\lambda - \kappa}\bar{p}_c' d\varepsilon_v^p \tag{5}$$

where υ is the specific volume; λ is the slope of conventional normal compression line in υ-ln p' plane; κ is the slope of reloading line in υ-ln p' plane; $d\varepsilon_v^p$ is the volumetric plastic strain increment.

Meanwhile, a progressive hardening law for dr is introduced with a generalized plastic strain to account for the contribution of both volumetric and shear plastic deformation parts. It should be noted that different strain types are considered in previous works [30, 31, 32]. Russell and Muir Wood [28] pointed out that the inclusion of both volumetric and shear parts was of paramount importance in accurately describing soil behavior. This hardening law reads as follows:

$$dr = \frac{\upsilon}{\lambda - \kappa} s(1-r) d\varepsilon_d^p = \frac{\upsilon}{\lambda - \kappa} s(1-r)\left(d\varepsilon_v^p + A_d d\varepsilon_s^p\right) \tag{6}$$

where s is the key material parameter ($s > 0$) that determines the rate at which the Loading surface hardens towards the Yield surface; A_d is a material parameter ($A_d > 0$) which controls the contribution of plastic shear strain to strain hardening.

As plotted in Fig.2(c), s controls the nonlinearity of the isotropic compression line in over-consolidated states in υ-ln p' plane. As s varies from 4 to 1000, the behavior switches from a nonlinear trend to a bi-loglinear behavior as in the modified cam-clay model. Calibrated with the test results of natural Boom clay, a value of 8 is found for s.

As plotted in Fig.2(d), parameter A_d ($A_d \geq 0$) can be obtained by fitting stress paths during drained softening stages in highly over-consolidated states. Parameter A_d describes how the plastic shear strain affects the hardening process. As A_d varies from 0 to 5, the nonlinearity on the 'dry side' is increasingly obvious. It is noteworthy that when $A_d = 0$, the plastic shear strain does not contribute to the hardening process anymore. The most suitable value of A_d for natural Boom clay

is 0.1.

The stress dilatancy relation proposed by McDowell et al. [19] is adopted to define a non-associated flow rule for better describing the volumetric strain and excess pore pressure generation during undrained loadings for natural stiff clays. Assuming a plastic potential having the same shape as the yield surfaces but a different pair of parameters (M_g, k_g), the stress dilatancy equation and the non-associated flow rule are expressed as follows:

$$\frac{d\varepsilon_v^p}{d\varepsilon_s^p}=\frac{\dfrac{\partial g_I}{\partial p}}{\dfrac{\partial g_I}{\partial q}}=\frac{M_g^2-\eta^2}{k_g\eta} \tag{7}$$

$$d\varepsilon_v^p=\Lambda\frac{\partial g_I}{\partial p},\quad d\varepsilon_s^p=\Lambda\frac{\partial g_I}{\partial q} \tag{8}$$

where η denotes the stress ratio q/p', M_g is the critical state ratio where no further volumetric strain develops and k_g controls the shape of the plastic potential and the direction of plastic flow. Fig.2(b) depicts the variation of plastic flow direction (k_g) from 0.5 to 2 in p'-q plane. The calibrated yielding behavior of natural Boom clay shows that the closest value of k_g is 0.9.

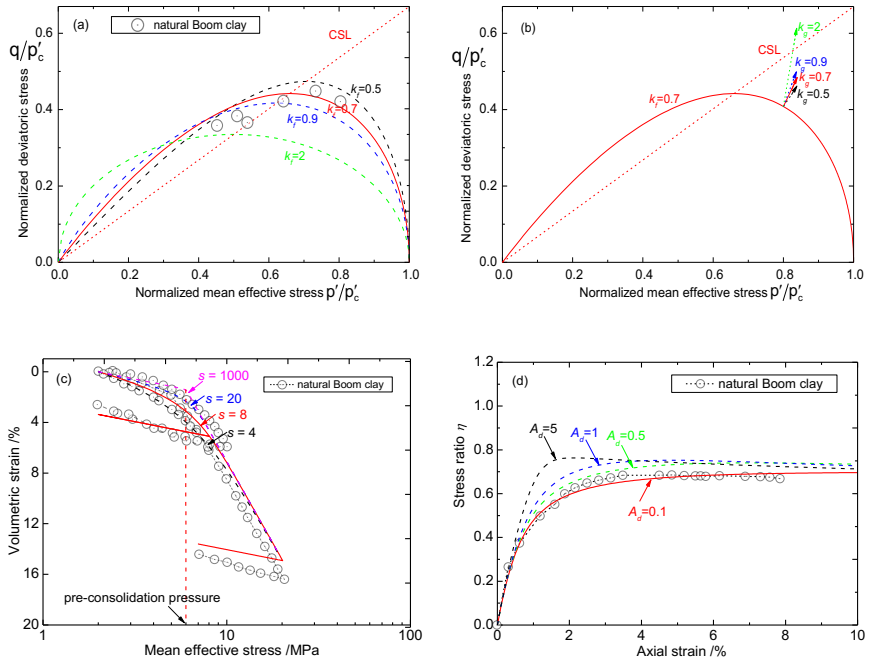

Fig.2 Variation of parameters of ACC2 model in p'-q plane and v-ln p' plane: (a) k_f varies from 0.5 to 2; (b) k_g varies from 0.5 to 2; (c) s varies from 4 to 1000; (d) A_d varies from 0.1 to 5

With eleven material parameters (five of them are the same as MCC model), the two-surface plasticity model named ACC2, similarly to bounding surface plasticity theory, has been proposed to consider the mechanical behavior of both normally consolidated and over-consolidated stiff clays. Five of them (λ, κ, $\overline{p}_c'$, v, M_f) are the same as for the modified cam-clay model. r denotes the inverse of over-consolidation ratio. Two parameters (k_f, k_g) control the shapes of the yield surface and the plastic potential surface. Two parameters (s, A_d) are used to account for a progressive hardening mechanism in over-consolidated states. Thus, the following discussion about ACC2 model is mainly done by considering four principal parameters, namely k_f (shape of yield surface), k_g (direction of plastic flow), s (isotropic compression nonlinearity) and A_d (deviatoric nonlinearity).

3. Problem statement

3.1 Undrained cylindrical cavity expansion/contraction

Fig.3 presents schematic plots of cylindrical cavity expansion/contraction problems with initial radius $a_{0,0}$ in an infinite elasto-plastic soil layer under undrained conditions. As the cavity expands or shrinks from initial radius $a_{0,0}$ to current radius a_0, a failure zone would be formed in the vicinity of the cavity wall. At the same time, the outside zone limited by radius $a_{x,0}$ would be plastic with stress points always lying on the Loading surface. Beyond that radius, the soil is in the elastic regime.

The radial equilibrium equation for cylindrical cavity expansion/contraction problem is expressed in terms of the effective stress as:

$$\frac{d\sigma_r'}{da_x}+\frac{\sigma_r'-\sigma_\theta'}{a_x}+\frac{du_w}{da_x}=0 \tag{9}$$

where σ_r', σ_θ' are radial, tangential effective stress of any material point, respectively. u_w stands for pore pressure.

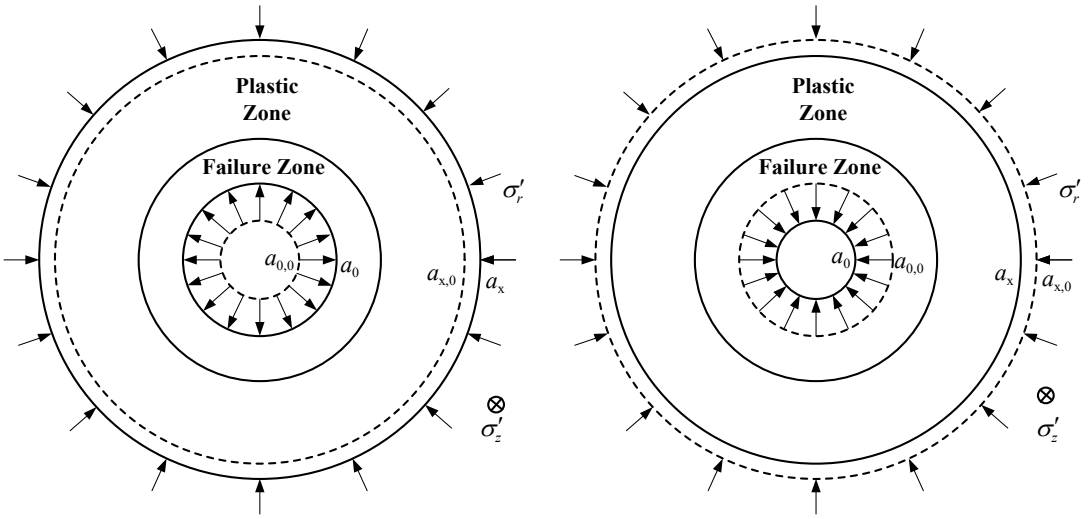

(a) (b)

Fig.3 Geometry of cylindrical cavity problem: (a) expansion; (b) contraction

Based on the compatibility condition and large deformation theory, a generalized logarithmic definition of strains in Eulerian description can be adopted in all areas [6]:

$$\varepsilon_r = -\ln(\frac{da_x}{da_{x0}}),\quad \varepsilon_\theta = -\ln(\frac{a_x}{a_{x0}}),\quad \varepsilon_v = -\ln(\frac{\upsilon}{\upsilon_0}) \tag{10}$$

where a_x, a_{x0} are the current and initial radii of any material points, respectively. ε_r, ε_θ, ε_v are the radial, tangential and volumetric strains, respectively. υ, υ_0 are the current and initial void ratios, respectively.

For further study, they can also be expressed in incremental form, as follows:

$$d\varepsilon_r = -\frac{\partial(da_x)}{\partial a_x},\quad d\varepsilon_\theta = -\frac{da_x}{a_x},\quad d\varepsilon_v = -\frac{d\upsilon}{\upsilon} \tag{11}$$

3.2 Elastoplastic analysis under undrained condition

The incremental stress-strain relationship for ACC-2 model is expressed in Lagrangian description (see A-17 in Appendix A):

$$\begin{bmatrix} D\sigma'_r \\ D\sigma'_\theta \\ D\sigma'_z \end{bmatrix} = \begin{bmatrix} c_{rr} & c_{r\theta} & c_{rz} \\ c_{\theta r} & c_{\theta\theta} & c_{\theta z} \\ c_{zr} & c_{z\theta} & c_{zz} \end{bmatrix} \begin{bmatrix} D\varepsilon_r \\ D\varepsilon_\theta \\ D\varepsilon_z \end{bmatrix} \tag{12}$$

where D denotes the differential of material points in Lagrangian description which should be distinguished from d in Eulerian form.

Under relatively low stress and undrained conditions, most analytical and semi-analytical solutions, including Chen and Abousleiman's method [9], consider the soil mixture as an incompressible material with the undrained Poisson's ratio being equal to 0.5 and the volumetric strain remaining constant. The volume change of pore water due to external loading is ignored. This is the case referred to as constant soil volume (CSV). Most reasonable analytical and semi-analytical solutions for undrained cavity problems are extensively developed and applied for various geotechnical problems based on this premise [6-9, 11-15]. Appendix B depicts the undrained solution in the form of five first-order ordinary differential equations for the comparative study. However, under high stress and low porosity conditions, the real compressibility of pore fluids (e. g water, oil) would exhibit a significant influence on the excess pore pressure and stress distribution along the cavity. This condition of constant soil volume can actually be relaxed by considering that undrained conditions correspond to a situation with constant soil mass (CSM).

The well-known Skempton coefficient B, which indicates the ratio between the change in pore pressure and the change in total applied stress in Appendix C-12, could also be used to illustrate the difference. For CSV premise, the value of B is always 1 in saturated conditions. This situation may be reasonable for soft clayey soils under low stress conditions (B>0.95), but not for stiff clays and soft claystone under high stress conditions (e.g. B≈0.92 for natural Boom clay [23], B≈0.75 to 0.84 for Callovo–Oxfordian claystone [24, 34], B≈0.88 for Opalinus argillite [25]). In such cases, the CSV assumption would lead to unavoidable computational errors for stress and pore pressure distributions, since the effect of pore fluids' compressibility under high stress conditions in not accounted for. Note that the compressibility of the solid particles is still neglected, since it leads to volume changes that are one order of magnitude (at least) lower than the compressibility of the pore fluid.

3.3 Undrained cavity expansion/contraction seen as constant soil mass conditions

In the framework of poro-elasto-plasticity theory, pore fluid is typically regarded as a compressible elastic medium with a large bulk modulus (e.g. 2.2×10^3 MPa for water, 1.6×10^3 MPa for oil at room temperature 20˚C and isotropic pressure 1 MPa), which is slightly sensitive to

temperature and pressure variations [21]. The bulk modulus of pore fluid is usually dozens of times that of solid grain. For most clays, the compressibility of solid grains can be neglected (e.g. C_s=2.0×10^{-5} MPa^{-1} for Illite [33], to be compared to the water compressibility C_w=45.5×10^{-5} MPa^{-1} for water). Considering infinitesimal transformation and undrained conditions (CSM), and neglecting solid grains compressibility, pore water pressure change and soil volumetric change are related using Eulerian porosity n and pore fluid's bulk modulus k_w (k_w=1/C_w) as follows:

$$du_w = \frac{d\varepsilon_v - C_s dp}{\phi\left(C_w - C_s\right)} \approx \frac{d\varepsilon_v}{nC_w} = \frac{k_w d\varepsilon_v}{n} \tag{13}$$

It is noteworthy that Eq (13) is deduced in the framework of poromechanics by Coussy [20]. More details are presented in Appendix C.

In analyses considering CSM, the soil volumetric strain increment at any material point cannot be ignored even under undrained condition. Meanwhile, the vertical strain increment is still null in cylindrical cavity analysis (plane strain conditions). The general incremental solution for cylindrical cavity problem is expressed in Lagrangian description, as follows:

$$D\varepsilon_v = -\frac{D\upsilon}{\upsilon}, \quad D\varepsilon_\theta = -\frac{Da_x}{a_x}, \quad D\varepsilon_z = 0 \tag{14}$$

An auxiliary independent variable ξ is chosen as the ratio of initial radial position to current radial position for each specific particle. The following differentiations can be done:

$$\xi = \frac{a_{x0}}{a_x}, \quad \frac{D\xi}{Da_x} = -\frac{a_{x0}}{a_x^2}, \quad \frac{D\varepsilon_\theta}{D\xi} = -\frac{Da_x}{a_x D\xi} = \frac{a_x}{a_{x0}} = \frac{1}{\xi} \tag{15}$$

Substituting Eq (15) into Eq (12), the incremental stress-strain relationship can be transformed into three first-order ordinary differential equations with an unknown Lagrangian-form differential $\frac{D\varepsilon_v}{D\xi}$:

$$\frac{D\sigma_r'}{D\xi} = c_{rr}\frac{D\varepsilon_v}{D\xi} + \frac{c_{r\theta} - c_{rr}}{\xi} \tag{16}$$

$$\frac{D\sigma_\theta'}{D\xi} = c_{\theta r}\frac{D\varepsilon_v}{D\xi} + \frac{c_{\theta\theta} - c_{\theta r}}{\xi} \tag{17}$$

$$\frac{D\sigma_z'}{D\xi} = c_{zr}\frac{D\varepsilon_v}{D\xi} + \frac{c_{z\theta} - c_{zr}}{\xi} \tag{18}$$

At the same time, the excess pore water pressure can be given in Lagrangian description:

$$Du_w = \frac{k_w}{n} D\varepsilon_v \tag{19}$$

Thus:

$$\frac{Du_w}{D\xi} = \frac{\upsilon k_w}{\upsilon - 1} \frac{D\varepsilon_v}{D\xi} \tag{20}$$

where k_w is the bulk modulus of pore water, n is the current porosity and υ is current specific volume.

In order to make the problem solvable, let us consider $\frac{D\varepsilon_v}{D\xi} = f$. Substitute Eq (16) and Eq (20) into the radial equilibrium equation (9) gives:

$$\left(\frac{D\sigma'_r}{D\xi} + \frac{Du_w}{D\xi} \right) \frac{d\xi}{da_x} + \frac{\sigma'_r - \sigma'_\theta}{a_x} = 0 \tag{21}$$

Unlike $\frac{D\xi}{Da_x}$ in Eq (15), $\frac{d\xi}{da_x}$ corresponds to a Eulerian description:

$$\frac{d\xi}{da_x} = \frac{\frac{da_{x0}}{da_x} a_x - a_{x0}}{a_x^2} = \frac{1}{a_x} \left(\frac{da_{x0}}{da_x} - \xi \right) = \frac{1}{a_x} \left(e^{\varepsilon_r} - \xi \right) \tag{22}$$

Integrating Eq (10), the full form of radial strain can be obtained:

$$\varepsilon_r = \varepsilon_v - \varepsilon_\theta = -\ln\left(\frac{\upsilon}{\upsilon_0} \right) + \ln\left(\frac{a_x}{a_{x0}} \right) = \ln\left(\frac{\upsilon_0}{\upsilon \xi} \right) \tag{23}$$

Then:

$$\frac{d\xi}{da_x} = \frac{1}{a_x} \left(\frac{\upsilon_0}{\upsilon \xi} - \xi \right) \tag{24}$$

Making full use of Eq (16), Eq (20) and Eq (24), the radial equilibrium equation (9) turns into Eq (25):

$$\left(c_{rr} f + \left(c_{r\theta} - c_{rr} \right) \frac{1}{\xi} + \frac{\upsilon k_w}{\upsilon - 1} f \right) \times \frac{1}{a_x} \left(\frac{\upsilon_0}{\upsilon \xi} - \xi \right) + \frac{\sigma'_r - \sigma'_\theta}{a_x} = 0 \tag{25}$$

Then, an equation relating f to the other principal variables σ'_r, σ'_θ, $c_{r\theta}$, c_{rr}, υ and ξ is obtained:

311 $$f=-\frac{\xi\left(\sigma_r'-\sigma_\theta'\right)+\left(\frac{\upsilon_0}{\upsilon\xi}-\xi\right)\left(c_{r\theta}-c_{rr}\right)}{\left(\frac{\upsilon_0}{\upsilon}-\xi^2\right)\left(c_{rr}+\frac{\upsilon k_w}{\upsilon-1}\right)} \tag{26}$$

312 The previous four first-order ordinary differential equations are finally reduced into a full
313 explicit form with respect to the auxiliary independent variable ξ:

314 $$\frac{D\sigma_r'}{D\xi}=c_{rr}f+\frac{c_{r\theta}-c_{rr}}{\xi} \tag{27}$$

315 $$\frac{D\sigma_\theta'}{D\xi}=c_{\theta r}f+\frac{c_{\theta\theta}-c_{\theta r}}{\xi} \tag{28}$$

316 $$\frac{D\sigma_z'}{D\xi}=c_{zr}f+\frac{c_{z\theta}-c_{zr}}{\xi} \tag{29}$$

317 $$\frac{Du_w}{D\xi}=\frac{\upsilon k_w}{\upsilon-1}f \tag{30}$$

318 The other three variables, namely specific volume υ, pre-consolidation pressure $\overline{p}_c'$ and
319 positive scalar r are also included in the differential equations through equation (26):

320 $$\frac{D\upsilon}{D\xi}=-\upsilon f \tag{31}$$

321 $$\frac{D\varepsilon_v^p}{D\xi}=\frac{D\varepsilon_v}{D\xi}-\frac{D\varepsilon_v^e}{D\xi}=f-\frac{\kappa}{\upsilon\left(\sigma_r'+\sigma_\theta'+\sigma_z'\right)}\left(\frac{D\sigma_r'}{D\xi}+\frac{D\sigma_\theta'}{D\xi}+\frac{D\sigma_z'}{D\xi}\right) \tag{32}$$

322 $$\frac{D\varepsilon_s^p}{D\xi}=\frac{D\varepsilon_s^p}{D\varepsilon_v^p}\frac{D\varepsilon_v^p}{D\xi}=\frac{k_g\eta}{M_g^2-\eta^2}\left[f-\frac{\kappa}{\upsilon\left(\sigma_r'+\sigma_\theta'+\sigma_z'\right)}\left(\frac{D\sigma_r'}{D\xi}+\frac{D\sigma_\theta'}{D\xi}+\frac{D\sigma_z'}{D\xi}\right)\right] \tag{33}$$

323 $$\frac{D\overline{p}_c'}{D\xi}=\frac{v}{\lambda-\kappa}\overline{p}_c'\frac{D\varepsilon_v^p}{D\xi}=\frac{\upsilon}{\lambda-\kappa}\overline{p}_c'\left[f-\frac{\kappa}{\upsilon\left(\sigma_r'+\sigma_\theta'+\sigma_z'\right)}\left(\left(c_{rr}+c_{\theta r}+c_{zr}\right)\left(f-\frac{1}{\xi}\right)+\frac{c_{r\theta}+c_{\theta\theta}+c_{z\theta}}{\xi}\right)\right] \tag{34}$$

324 $$\begin{aligned}\frac{Dr}{D\xi}&=\frac{\upsilon}{\lambda-\kappa}s\left(1-r\right)\left(\frac{D\varepsilon_v^p}{D\xi}+A_d\frac{D\varepsilon_s^p}{D\xi}\right)\\&=\frac{\upsilon}{\lambda-\kappa}s\left(1-r\right)\left(1+A_d\frac{k_g\eta}{M_g^2-\eta^2}\right)\left[f-\frac{\kappa}{\upsilon\left(\sigma_r'+\sigma_\theta'+\sigma_z'\right)}\left(\left(c_{rr}+c_{\theta r}+c_{zr}\right)\left(f-\frac{1}{\xi}\right)+\frac{c_{r\theta}+c_{\theta\theta}+c_{z\theta}}{\xi}\right)\right]\end{aligned} \tag{35}$$

325 At this stage, based on the premise of CSM, the cylindrical cavity expansion/contraction
326 problem under undrained conditions is finally reduced to seven ordinary differential equations (Eq
327 (27), Eq (28), Eq (29), Eq (30), Eq (31), Eq (34), Eq (35)). These equations can be solved as an

initial boundary value problem with ξ starting from 1. It is worth noting that these ordinary differential equations which are expressed in terms of ξ should finally be converted to the radius position a_x. From equation (24), it is obtained:

$$\frac{da_x}{a_x} = \frac{d\xi}{\frac{\upsilon_0}{\upsilon\xi} - \xi} \tag{36}$$

Integrating the above equation, the following formula is obtained:

$$\frac{a_x}{a_0} = \exp\left(\int_{\xi(a_0)}^{\xi} \frac{d\xi}{\frac{\upsilon_0}{\upsilon\xi} - \xi} \right) \tag{37}$$

3.4 Initial condition

The classical undrained cylindrical cavity expansion/contraction problem is eventually solved using these seven first-order ordinary differential equations with the corresponding initial stress conditions. These stress conditions are initially defined as:

$$\sigma'_r(a_{x0}) = \sigma'_{r0}, \quad \sigma'_\theta(a_{x0}) = \sigma'_{\theta 0}, \quad \sigma'_z(a_{x0}) = \sigma'_{z0}, \quad u_w(a_{x0}) = u_{w0}, \quad \upsilon(a_{x0}) = \upsilon_0, \quad p'_c(a_{x0}) = p'_{c0},$$

$$r(a_{x0}) = r_0$$

4. Results and discussion

In this section, the results obtained from the semi-analytical solution are presented for the cylindrical cavity expansion/contraction in soils under undrained conditions. The original 11 material parameters of ACC2 model are calibrated and chosen by fitting the laboratory test (isotropic compression, drained triaxial compression) results for natural Boom Clay according to Hong et al. [16] (Table 1 and Table 2): υ_s (void ratio in critical state at isotropic stress of 1 MPa) = 1.84, λ (slope of normal consolidation line in υ-ln p' plane) = 0.18, κ (slope of unloading line in υ-ln p' plane) = 0.02, M_g (critical state ratio) = 0.67, M_f (stress ratio at apex of yield surface)= 0.67, $\overline{p}'_c$ (pre-consolidated pressure) = 6 MPa. The Poisson ratio ν is assumed to be 0.3. It should be noted that the calibration process could be improved by an appropriate genetic algorithm which has been studied in previous literatures [40-45].

The undrained shear strength s_u is calculated based on the premise of constant soil volume (Wood, 1990):

$$s_u = \frac{1}{\sqrt{3}} M_g \mathrm{e}^{(\upsilon_s - \upsilon_0)/\lambda} \tag{38}$$

As mentioned previously, under undrained loading process, the soil sample at low void ratio and under high stress would also induce a slight volumetric strain increment which explains the variation of pore pressure. The s_u assumed here is only for the nondimensionalization purpose.

This section firstly highlights the effect of the compressibility of pore fluid and the importance of solving the cavity expansion problem using poro-elasto-plasticity under various stress conditions. Representative comparisons are given in Fig. 4-6 between the results for normally consolidated soils based on constant soil volume (CSV) and constant soil mass (CSM) conditions at isotropic effective stresses of 2 MPa, 10 MPa, 50 MPa, respectively. The soil mass is fully saturated with pore water. Moreover, a full range of isotropic stresses from 0.1 MPa to 100 MPa is considered to assess the relative errors between these two assumptions under cavity expansion condition ($a_0/a_{0,0} = 2$). Isoerror maps computed for stress components are plotted in Fig. 7.

Then, based on CSM premises, parametric studies of cavity expansion at normal consolidated stress state (r=1) and highly over-consolidated stress state (r=2.9) using ACC2 model are conducted. It aims at illustrating the advantages brought by the use of this sophisticated model, when compared to simple models like MCC, for which analytical solutions for the same problem already exist.

(1) ACC2 model with different values of yield shape parameter k_f (0.5 to 2) as Case 4 and plastic flow direction parameter k_g (0.5 to 2) as Case 5 at normally consolidated stress state (r_0=1) is applied to investigate the effect of the shape of yield surface (the yielding behavior) and the shape of plastic potential surface (the direction of plastic flow).

(2) ACC2 model with isotropic compression non-linearity parameter s (4 to 1000) as Case 6 and deviatoric non-linearity parameter A_d (0.1 to 5) as Case 7 is applied to investigate the effect of the nonlinearity at a highly over-consolidated stress state (r_0=2.9).

4.1 Comparison between CSV and CSM conditions

The results obtained using CSV and CSM assumptions at three isotropic effective stress states (p'=2, 10, 50 MPa) are compared in Fig. 4 as Case 1, Fig. 5 as Case 2 and Fig. 6 as Case 3. The soil is initially assumed to be at normally consolidated and isotropic stress state (r=1), then rapidly expanded to a certain cavity radius ($a_0/a_{0,0}$ = 2) without considering the rate and seepage effect. During the expanding process, a critical state zone where the stress state at any point satisfies $q=M_g p'$ would be formed in vicinity of the cavity. Outside the critical state zone, all material points reach the plastic state to some extent.

There is a clear difference between CSV and CSM in stress and excess pore pressure distributions along the radius distance in Fig. 4-6. From the normalized effective stress (σ_r'/s_u, σ_θ'/s_u, σ_z'/s_u) distributions along the radius distance corresponding to the cavity radius ratio of $a_0/a_{0,0}$ = 2 in Fig. 4(a), Fig. 5(a) and Fig. 6(a), the expanding results obtained based on CSM appear to be slightly larger than those based on CSV at each corresponding point. The opposite phenomenon could be observed in the normalized excess pore pressure $\Delta u_w/s_u$ and stress ratio η distributions along the radius distance in Fig. 4(b), Fig. 5(b) and Fig. 6(b). Meanwhile, the range of critical state zone (see CP boundary) for CSM is shorter than for CSV. The CP boundary corresponds to the boundary between critical state zone and plastic zone. It can be determined by the evolution of current stress ratio (η=q/p') along normalized radial distance. With the increase of initial isotropic stress, the difference between CSV and CSM becomes more and more obvious. Through the comparison between the two cases, it can be concluded that the premise of CSV would influence the excess pore pressure and principal effective stress distributions. This confirms the necessity of considering the compressibility of pore fluid under high stress conditions.

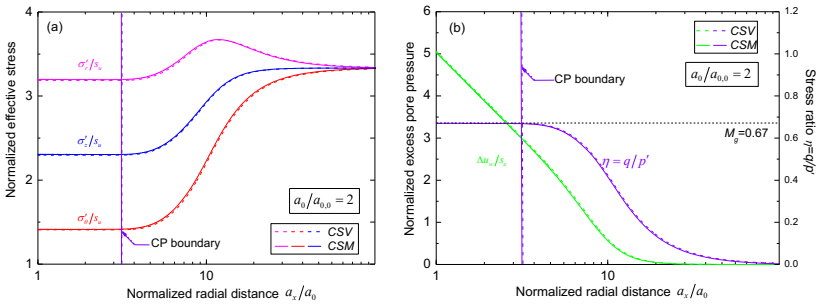

Fig. 4 Undrained cavity expansion at normally consolidated and isotropic stress state (p'= 2 MPa):

(a) normalized principal stress distributions; (b) normalized excess pore pressure and stress ratio distribution

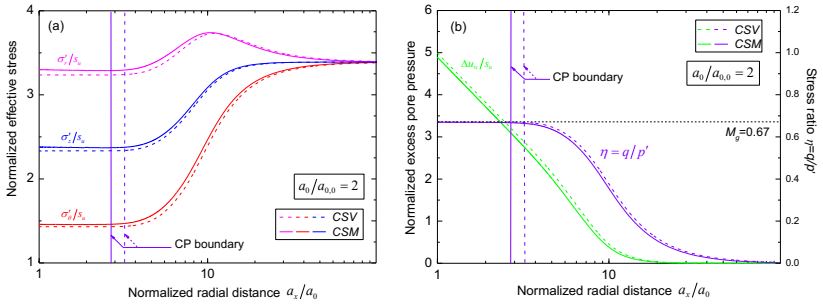

Fig. 5 Undrained cavity expansion at normally consolidated and isotropic stress state (p'= 10 MPa): (a) normalized principal stress distributions; (b) normalized excess pore pressure and stress ratio distribution

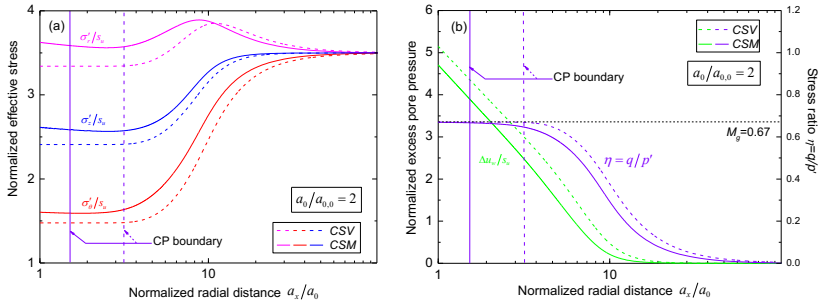

Fig. 6 Undrained cavity expansion at normally consolidated and isotropic stress state (p'= 50 MPa): (a) normalized principal stress distributions; (b) normalized excess pore pressure and stress ratio distribution

In order to estimate the relative errors based on the two premises, a full range of isotropic stress from 0.1 MPa to 100 MPa is considered in cavity expansion process. The relative errors (Re) for three principal stresses and pore pressure are defined as: $Re = |V_{CSM} - V_{CSV}|/|V_{CSM}|$. In the formula, V_{CSM}, V_{CSV} represent the corresponding results of each material point based on CSM and CSV, respectively.

421

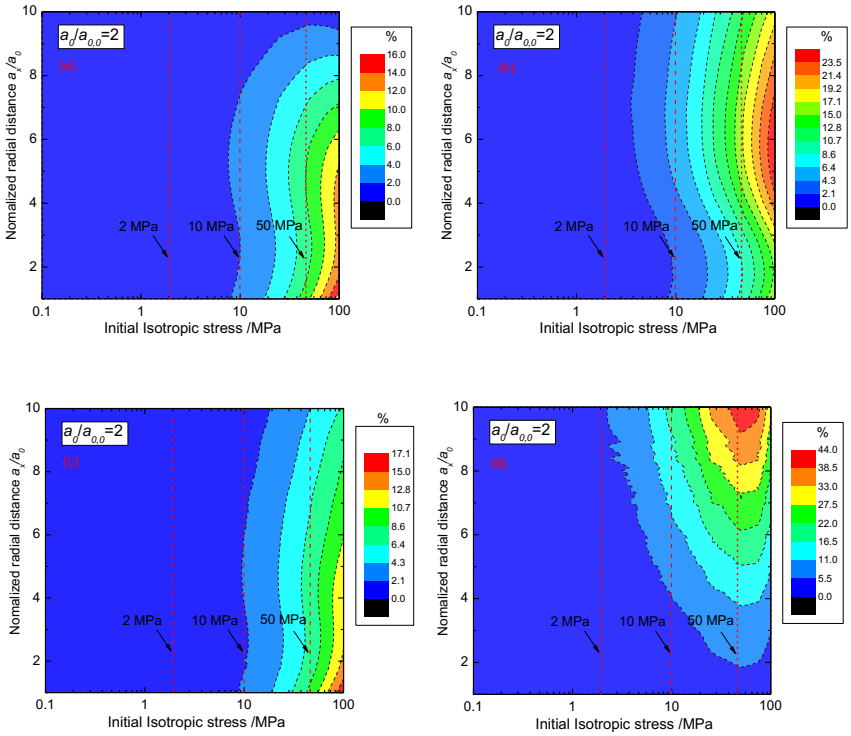

422

423 Fig. 7 Isoerror maps plotted for constant soil mass (CSM) and constant soil volume (CSV): (a)
424 radial effective stress; (b) tangential effective stress; (c) vertical effective stress; (d) excess pore
425 pressure

426 Figs. 7(a)-(c) plot isoerror maps for the three principal effective stress distributions from a_x/a_0
427 = 1 to a_x/a_0 = 10 in mean effective stress range from 0.1 MPa to 100 MPa when the cavity expands
428 to $a_0/a_{0,0}$ = 2. Case 1 of p'=2 MPa, case 2 of p'=10 MPa, case 3 of p'=50 MPa are specially pointed
429 out. In the range from 0.1 MPa to 1 MPa (low stress conditions), the value of *Re* is less than 1%,
430 suggesting that both cases (CSM, CSV) would get reliable results in principal stress distributions.
431 However, when the isotropic stress is larger than 10 MPa (relatively high stress conditions), the
432 value of *Re* would increase rapidly. Meanwhile, the *Re* value for excess pore pressure distribution
433 in Fig. 7(d) is much more sensitive to pressure change than the effective stress distribution at both
434 low and high stress conditions.

435 Thus, for the applications focusing on the evolution of excess pore pressure, CSM would be a
436 preferential choice for solving the cavity expansion problems even under low stress conditions.

437

438 **4.2 Results with variations of yield surface parameter**

439 A parametric study of cavity expansion is presented as Case 4 with variable k_f and fixed k_g (k_g =
440 0.9) for r=1 (normally consolidated state) based on CSM. Four different values of k_f (0.5, 0.7, 0.9,
441 2), representing tear shape to elliptical shape, are considered to investigate the impact of the shape
442 of yield surface on the stress and pore pressure distributions around the cavity.

443 Fig. 8(a) shows the effective stress paths normalized by the undrained shear strength s_u from
444 $a_0/a_{0,0}$ = 1 to $a_0/a_{0,0}$ = 2 at the cavity wall. With the change of k_f from 0.5 to 2, the shape of yield
445 surface varies and the intersection with the critical state line decreases. Figs. 8(b), 8(d) depict the
446 normalized effective stresses (σ'_r/s_u, σ'_θ/s_u, σ'_z/s_u) and pore pressure $\Delta u_w/s_u$ distributions
447 along radius position. The radius position a_x is normalized by cavity radius a_0 and plotted in the
448 scale of logarithm. It can be seen that in the vicinity of cavity wall the three principal stresses
449 remain almost unchanged, indicating that the soil in this range has reached the critical state.

450 Further investigation on the shape variation of yield surface shows that positive increment of
451 k_f would sharply decrease the values of the three principal stresses in the critical state range (Fig.
452 8(a)), but have negligible effects on the location of CP boundary. Fig. 8(c) presents the cylindrical
453 cavity expansion curve from $a_0/a_{0,0}$ = 1 to $a_0/a_{0,0}$ = 10 at the cavity wall. The cavity pressure and
454 excess pore pressure increase rapidly to a limit and then stay constant with cavity expanding. With
455 the change of k_f from 0.5 to 2, the present solution predicts a decreasing cavity pressure and excess
456 pore pressure limit around cavity wall. In Fig. 8(d), the normalized excess pore pressure would
457 decrease monotonously along the radial distance. In the vicinity of the cavity wall, the stress point
458 would reaches the critical state where three principal stresses (σ'_r, σ'_θ, σ'_z) remain almost
459 constant ($\frac{d\sigma'_r}{da_x}=\frac{d\sigma'_\theta}{da_x}=\frac{d\sigma'_z}{da_x}=0$) and the radial balance equation ($\frac{d\sigma'_r}{da_x}+\frac{\sigma'_r-\sigma'_\theta}{a_x}+\frac{du_w}{da_x}=0$)
460 would reduce into $\frac{\sigma'_{rc}-\sigma'_{\theta c}}{a_x}+\frac{du_w}{da_x}=0$. σ'_{rc}, $\sigma'_{\theta c}$ is the corresponding radial, tangential
461 effective stress at the critial state zone, respectively. So the solution of pore water pressure at this
462 zone would be $u_w=-\left(\sigma'_{rc}-\sigma'_{\theta c}\right)\ln a_x+C$(C is a constant). For the case of cavity expansion,
463 σ'_{rc} is larger than $\sigma'_{\theta c}$ and the excess pore pressure would decrease in the vicinity of the cavity
464 wall (critical state zone). Meanwhile, under normal consolidated state, the stress would directly

turn into shear contraction state before reaching the cirtical state line. So the excess pore pressure would directly decrease from CP boundary to $a_x/a_0 = 100$.

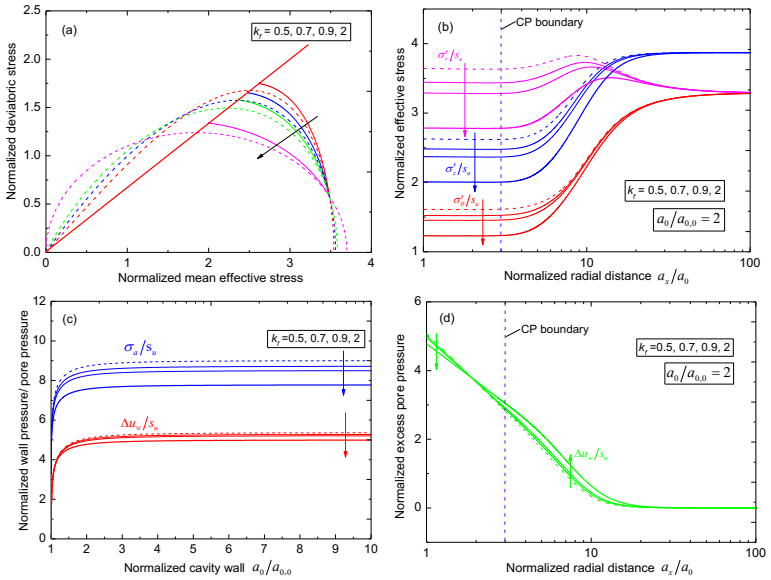

Fig. 8 Undrained cavity expansion results with change of k_f from 0.5 to 2: (a) normalized stress paths at cavity wall; (b) normalized principal stress distributions; (c) normalized cavity expansion curve; (d) normalized excess pore pressure distribution

4.3 Results with variations of plastic potential surface parameter

A parametric study is presented as Case 5 with variable k_g and fixed k_f (k_f = 0.7) for r=1 and $\bar{p}'_c$ (normally consolidated state) to investigate the impact of the direction of plastic flow on the stress and pore pressure distributions around the cavity.

From the same initial stress state, the four effective stress paths with different k_g values (0.5, 0.7, 0.9, 2) normalized by the undrained shear strength s_u from $a_0/a_{0,0}$ = 1 to $a_0/a_{0,0}$ = 2 at the cavity wall are found to be almost overlapped in Fig. 9(a). This suggests that k_g merely control the direction of plastic flow and portion of shear plastic strain in loading process. Fig. 9(b), 9(d) depict the normalized effective stresses (σ'_r/s_u, σ'_θ/s_u, σ'_z/s_u) and pore pressure $\Delta u_w/s_u$ distributions with the variation of k_g. The effective stresses in the vicinity of cavity wall typically remain constant. As opposed to changes of k_f, the direction variation of plastic flow shows that an positive increment of k_g induces more deviatoric plastic strains, leading to a sharp decrease of the

radius of critical state zone, but has negligible effects on the critical values of the three principal stresses in the critical state zone. It also shows a slight reduction of excess pore pressure around the cavity wall when an increasing plastic shear strain portion is produced.

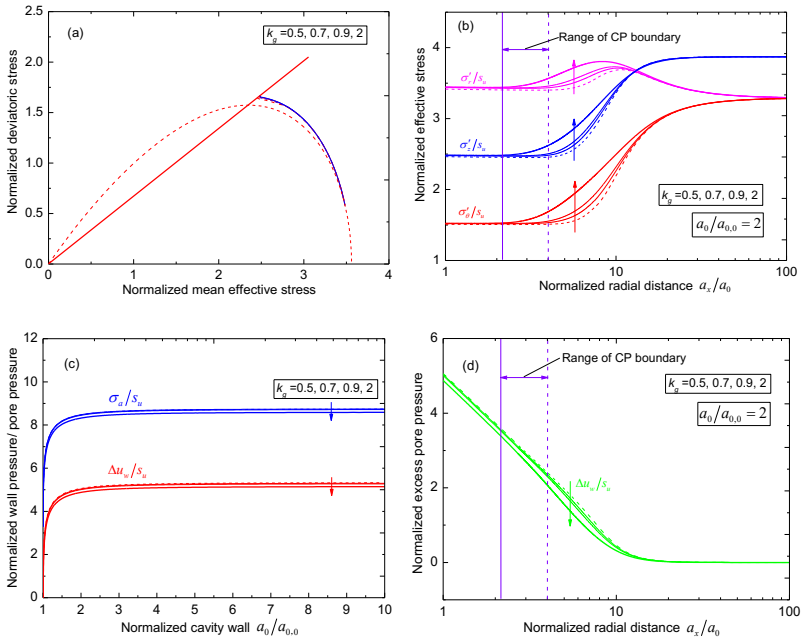

Fig. 9 Undrained cavity expansion results with the variation of k_g from 0.5 to 2: (a) normalized stress paths at cavity wall; (b) normalized principal stress distributions; (c) normalized cavity expansion curve; (d) normalized excess pore pressure distribution

4.4 Results with variations of isotropic nonlinear parameter

In highly over-consolidated states, stiff clays typically exhibit a non-linear behavior under loading process without pure elastic deformations. A parametric study of cavity expansion in over-consolidated states with different isotropic nonlinear parameter s (4, 8, 20, 1000) is presented as Case 6. Note that s controls the evolution rate of Loading surface in approaching Yield surface, namely the nonlinearity of isotropic compression from over-consolidated state to normally consolidated state. A smaller s represents a clear nonlinearity of isotropic loading in v-ln p' plane, while a larger s means that the compression line in v-ln p' plane is closer to bi-linearity.

The expanding cavity is defined by an initial in-situ stress of σ'_r=1.91 MPa, σ'_θ=1.91 MPa and σ'_z=2.25 MPa with a pre-consolidation pressure of $\bar{p}'_c$=6 MPa and over-consolidation ratio

of r=2.9 as listed in Table.2. Figs. 10(a)-(d) depict the normalized effective stress paths at cavity wall, normalized cavity expansion curves, the normalized effective stresses and excess pore pressure distributions with change of s. Under the expanding process from $a_0/a_{0,0}$ = 1 to $a_0/a_{0,0}$ = 2, the normalized effective stresses follow different stress paths with s varying from 4 to 1000 in Fig. 10(a). The direction of arrow means the increasing trend of s. When s reaches the value of 1000, the initial mechanical behavior is more elastic which explains the stress path being upward at the beginning of undrained loading process.

In Fig. 10(b), the range of critical state zone is sharply dependent on s. But the critical values of normalized effective stresses are independent of s. It is worth noting that with the decreasing of s (the increasing nonlinearity of isotropic compression), the radius of critical state zone would decrease to zero where no pure critical state zone exists. With the increasing of s (the decreasing nonlinearity of isotropic compression), the radius of critical state zone would increase to a limit where no further critical state zone develops. For an extremely large value of s (e.g. 1000), the analytical results are similar to the case of over-consolidated states expressed in modified cam-clay model [9]. Meanwhile, the increase in nonlinearity of isotropic compression would eventually results in the decrease of effective stress in plastic zone.

In Figs. 10(c)-(d), the normalized wall pressure at cavity wall is positive, in agreement with the value of s. A sophisticated phenomenon is observed on the normalized excess pore pressure. At the beginning of expanding process, the normalized excess pore pressure would firstly increase, decrease and then increase to a limited value. With the increasing of s, the increasing and decreasing phenomenon would be more obvious. At the expanded cavity of $a_0/a_{0,0}$ = 2, the normalized excess pore pressure at cavity wall would increase to a limit value with increasing s. In the critical state zone, the normalized excess pore pressure would decrease along the normalized radial distance. Unlike the results by modified cam-clay model [9], a ‘second peak’ of normalized excess pore pressure is observed, which is owing to the soil’s shear dilatancy behavior under highly over-consolidated states. From $a_x/a_0 = 100$ to the ‘second peak’, the excess pore pressure would increase (shear contraction); from the ‘second peak’ to the CP boundary, the excess pore pressure would decrease (shear dilatancy) and the value of excess pore pressure would be $-\left(\sigma'_{rc}-\sigma'_{\theta c}\right)\ln a_x + C$(C is a constant) in the range of critical state zone. The position of the

533 'second peak' is also consistent with the value of *s*. In the far end of expanded cavity, excess pore
534 pressure would vanish.

535

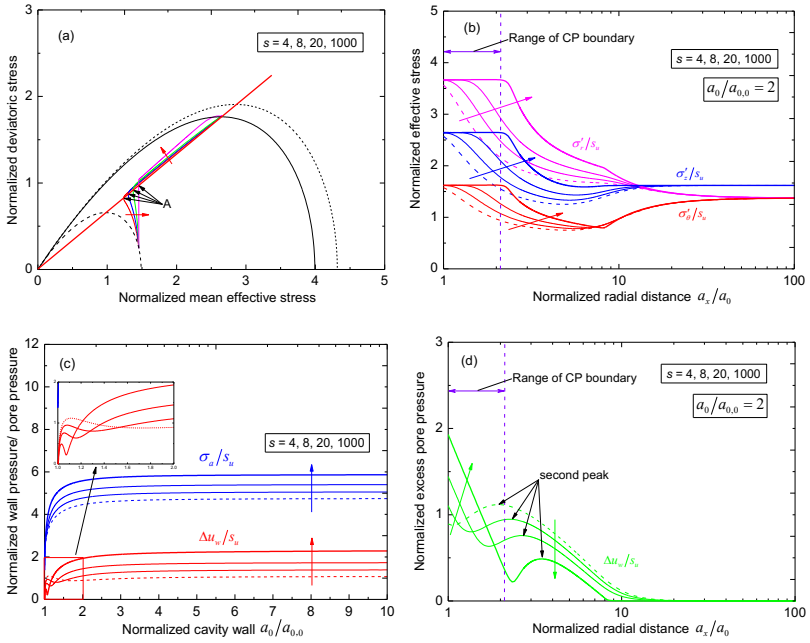

536

537 Fig. 10 Undrained cavity expansion results with different values of *s* from 4 to 1000: (a)
538 normalized stress paths at cavity wall; (b) normalized principal stress distributions; (c) normalized
539 cavity expansion curve; (d) normalized excess pore pressure distribution

540

541 **4.5 Results with the variations of deviatoric nonlinear parameter**

542 In over-consolidated states, parameter A_d describes how the plastic shear strain affects the
543 hardening process. It can be calibrated from the stress paths under high over-consolidated states in
544 undrained conditions. A parametric study of cavity expansion in over-consolidated states with
545 different values of deviatoric nonlinear parameter A_d (0.1, 0.5, 1, 5) is presented as Case 7.

546 An in-situ stress of σ_r' =1.91 MPa, σ_θ' =1.91 MPa and σ_z' =2.25 MPa with a
547 pre-consolidation pressure of $\bar{p}_c'$=6 MPa and over-consolidation ratio of *r*=2.9 is considered to
548 evaluate the impact of A_d on the stress and pore pressure distributions around the cavity.

549

550

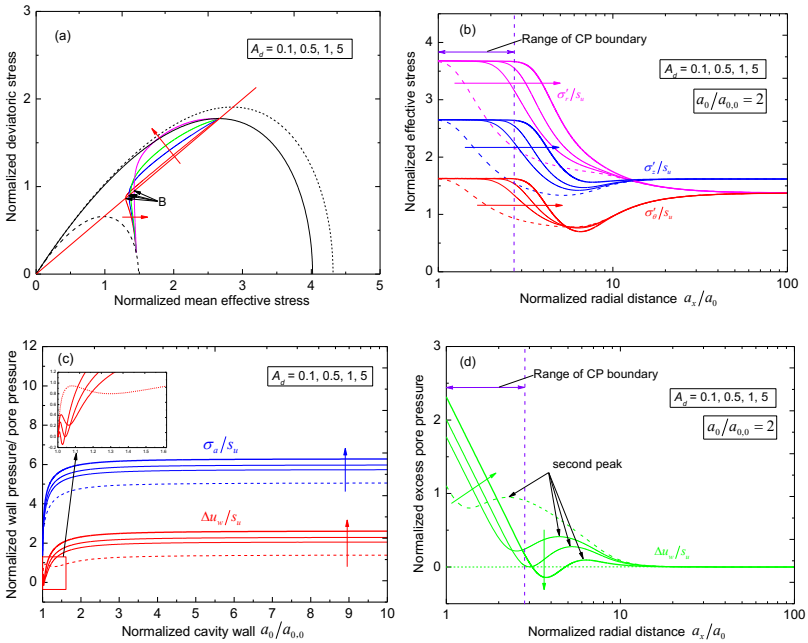

551 Fig. 11 Undrained cavity expansion results with different values of A_d from 0.1 to 5: (a)
552 normalized stress paths at cavity wall; (b) normalized principal stress distributions; (c) normalized
553 cavity expansion curve; (d) normalized excess pore pressure distribution

554 Figs. 11(a)-(d) depict the results with different A_d values. Similar to nonlinear parameter s,
555 the radius of critical state zone is sharply dependent on A_d. But the critical values of normalized
556 effective stress are independent of A_d. With the decreasing of A_d, the radius of critical state zone
557 would decrease to zero where no pure critical state zone exists. At the expanded cavity of $a_0/a_{0,0}$ =
558 2, the normalized excess pore pressure at the cavity wall and the range of critical state zone would
559 increase with increasing A_d. One should also note that the increasing of A_d means the increasing
560 portion of plastic shear strain and the decreasing portion of plastic volumetric strain in hardening
561 process. With the increasing of A_d, the stress path would be more likely upward at the beginning of
562 undrained loading process. In Fig. 11(d), a 'second peak' of normalized excess pore pressure is
563 also observed and the peak gradually vanish with the increasing of A_d.

564

565 ## 5. Application to Praclay Gallery excavation

566 This section examines the application of the present solution into the excavation of Praclay
567 Gallery in underground research facility HADES-URF built at a depth of 223m in natural Boom

clay and located in Mol, Belgium [26, 27]. The natural Boom clay is a deposit of over-consolidated stiff clay which have been specifically investigated in the previous studies [16]. Meanwhile, the natural Boom clay is initially considered as homogeneous, at an isotropic effective stress of 2.3 MPa and fully saturated with an initial pore pressure of 2.2 MPa.

Praclay Gallery is excavated 45 meters long in horizontal plane, so it is regarded as a plane strain problem as plotted in Fig. 12. The inner radius of Praclay Gallery and the thickness of the concrete liner is equal to 0.95 m, 0.3m, respectively. During the construction of Praclay Gallery, a total over-excavation of 0.06m is applied. Since it is finished in a short period (less than 1 day) and the intrinsic permeability of natural Boom clay is extremely low ($2\sim4\times10^{-19}$ m^2), the excavation of Praclay Gallery can also be regarded as an undrained cavity contraction process.

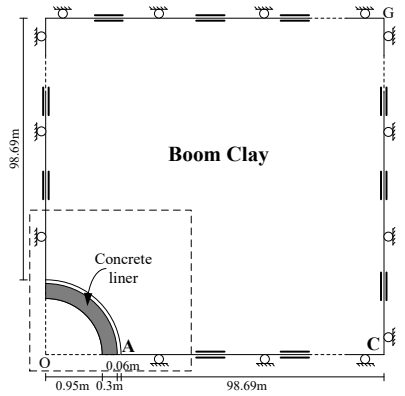

Fig. 12 Excavation plane of Praclay Gallery in natural Boom clay

Fig. 13(a) presents the analytical results by cavity contraction and the test values from four pore pressure transducers placed at different nominal radial distances from the center of Praclay Gallery [26]. It shows that the present solution could basically describe the pore pressure distribution along radial distances. In the vicinity of cavity wall, pore pressure would reduce with radial distance decreasing. Then a peak value shows up around the radial distance of 5~10m. After that peak, the pore pressure would gradually reduce to its normal value of 2.2 MPa.

Fig. 13(b) depicts three principal stress distributions along radial distance by the solution of cavity contraction. It shows that the vicinity of cavity wall has not reached the critical state yet. The effective stress path of point A in Fig. 13(c) can also be preferential for studying the stress states around the contracting wall.

In the cavity contraction curve (Fig. 13(d)), the wall pressure at Praclay Gallery would

gradually reduce with the increasing radial strain. In the present case, the radial strain is equal to 4.58% (radial displacement is 0.06m) and a wall pressure of 1.93 MPa is formed. However, when the radial strain reaches 21%, the wall pressure would be zero. It indicates that no more supporting pressure needs to be added on the cavity wall.

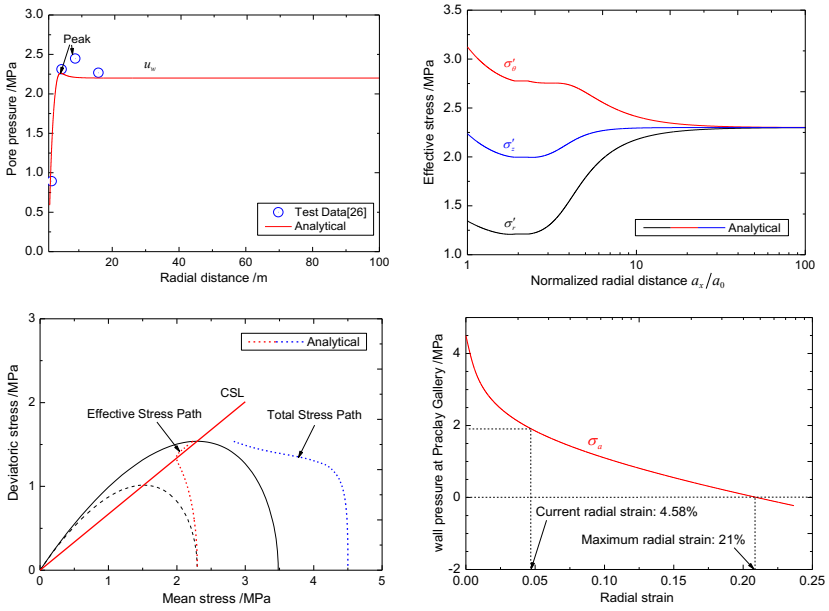

Fig. 13 The excavation of Praclay Gallery: (a) pore pressure distribution along radial distance; (b) principal effective stress distributions along normalized radial distance; (c) total and effective stress paths of Point A; (d) cavity contraction curve

6. Conclusion

This paper presents a semi-analytical solution for undrained cylindrical cavity expansion/contraction problems using a two-surface plasticity model, which can well reproduce the yielding behaviors, unassociated plastic flowing directions and high nonlinearity of stiff clays. To develop the new solution, the premise of constant soil mass based on poromechanics is recalled. A set of seven governing differential equations is obtained and solved as an initial boundary value problem with an auxiliary independent variable ξ. The new solution based on constant soil mass is then compared with the one based on constant soil volume, showing its relevance under high stress conditions. Then, based on the constant soil mass premise, the variations of yield surface parameter, plastic flow direction parameter, isotropic nonlinear parameter and deviatoric nonlinear

parameter are investigated in a parametric study focusing on the stress paths, stress and excess pore pressure distributions and cavity expansion/contraction curves. The results obtained allows the following conclusion to be drawn:

(1) The premise of constant soil mass is important in solving cavity expansion/contraction problems especially under high stress, low porosity and multi-fluid situations. Indeed, under relatively low stress conditions (e.g. p'<1 MPa), the solutions based on constant soil mass and constant soil volume are found to be similar. However, with the increasing of stress, the compressibility of pore fluid becomes crucial and the volumetric strain could be no longer regarded as constant. The premise of constant soil mass become preferential.

(2) In normally consolidated states, the shape variation of yield surface (k_f) would change the three principal stresses in critical state zone but have no effect on the range of critical state zone. On the contrary, the variation of plastic flow direction (k_g) would change the range of critical state zone but have no effect on the three principal stresses in the critical state zone.

(3) The high nonlinearity means no pure elastic zones in over-consolidated states. The decreasing of both nonlinearity parameter s and A_d decreases the range of critical state zone even to zero where no pure critical state zone exists. Meanwhile, a 'second peak' value of normalized excess pore pressure along cavity radius is observed and the peak would gradually approach the cavity wall with the decreasing of s and A_d.

(4) The present semi-analytical solution can be directly applied to explore the pore pressure, stress distributions and wall pressure around the expanding/contracting cavity (e.g. Praclay Gallery excavation).

Acknowledgements

The authors wish to acknowledge the support of National Natural Science Foundation of China (51938005) and the European Commission by the Marie Skłodowska-Curie Actions HERCULES-Towards Geohazards Resilient Infrastructure Under Changing Climates (H2020-500 MSCA-RISE-2017, 778360)

640 **Appendix A**

641 The effective stress and total strain increments are defined with three principal components in a
642 cylindrical coordinate system:

643 $$\mathbf{d\sigma'} = \begin{bmatrix} d\sigma'_r & d\sigma'_\theta & d\sigma'_z \end{bmatrix}^T \quad \text{(A - 1)}$$

644 $$\mathbf{d\varepsilon} = \begin{bmatrix} d\varepsilon_r & d\varepsilon_\theta & d\varepsilon_z \end{bmatrix}^T \quad \text{(A - 2)}$$

645 The total strain increment is split into elastic and plastic parts:

646 $$\mathbf{d\varepsilon} = \mathbf{d\varepsilon^e} + \mathbf{d\varepsilon^p} \quad \text{(A - 3)}$$

647 $$\mathbf{d\varepsilon^e} = \begin{bmatrix} d\varepsilon_r^e & d\varepsilon_\theta^e & d\varepsilon_z^e \end{bmatrix}^T \quad \text{(A - 4)}$$

648 $$\mathbf{d\varepsilon^p} = \begin{bmatrix} d\varepsilon_r^p & d\varepsilon_\theta^p & d\varepsilon_z^p \end{bmatrix}^T \quad \text{(A - 5)}$$

649 $$\boldsymbol{\alpha} = \begin{bmatrix} a_r & a_\theta & a_z \end{bmatrix}^T \quad \text{(A - 6)}$$

650 $$a_r = \frac{\partial f_1}{\partial \sigma'_r} = \frac{M_f^2}{3(1-k_f)}\left(\tfrac{2}{k_f}\, p'^{\frac{2}{k_f}-1}\left(rp'_c\right)^{2-\frac{2}{k_f}} - 2p'\right) + 6\left(\sigma'_r - p'\right) \quad \text{(A - 7)}$$

651 $$a_\theta = \frac{\partial f_1}{\partial \sigma'_\theta} = \frac{M_f^2}{3(1-k_f)}\left(\tfrac{2}{k_f}\, p'^{\frac{2}{k_f}-1}\left(rp'_c\right)^{2-\frac{2}{k_f}} - 2p'\right) + 6\left(\sigma'_\theta - p'\right) \quad \text{(A - 8)}$$

652 $$a_z = \frac{\partial f_1}{\partial \sigma'_z} = \frac{M_f^2}{3(1-k_f)}\left(\tfrac{2}{k_f}\, p'^{\frac{2}{k_f}-1}\left(rp'_c\right)^{2-\frac{2}{k_f}} - 2p'\right) + 6\left(\sigma'_z - p'\right) \quad \text{(A - 9)}$$

653 $$\mathbf{b} = \begin{bmatrix} b_r & b_\theta & b_z \end{bmatrix}^T \quad \text{(A - 10)}$$

654 $$b_r = \left(\frac{\partial g}{\partial p'} \Big/ \frac{\partial g}{\partial q} \times \frac{\partial p'}{\partial \sigma'_r} + \frac{\partial q}{\partial \sigma'_r}\right) \times k_g \eta = \frac{1}{3}\left(M_g^2 - \eta^2\right) + \frac{3}{q} k_g \eta \left(\sigma'_r - p'\right) \quad \text{(A - 11)}$$

655 $$b_\theta = \left(\frac{\partial g}{\partial p'} \Big/ \frac{\partial g}{\partial q} \times \frac{\partial p'}{\partial \sigma'_\theta} + \frac{\partial q}{\partial \sigma'_\theta}\right) \times k_g \eta = \frac{1}{3}\left(M_g^2 - \eta^2\right) + \frac{3}{q} k_g \eta \left(\sigma'_\theta - p'\right) \quad \text{(A - 12)}$$

656 $$b_z = \left(\frac{\partial g}{\partial p'} \Big/ \frac{\partial g}{\partial q} \times \frac{\partial p'}{\partial \sigma'_z} + \frac{\partial q}{\partial \sigma'_z}\right) \times k_g \eta = \frac{1}{3}\left(M_g^2 - \eta^2\right) + \frac{3}{q} k_g \eta \left(\sigma'_z - p'\right) \quad \text{(A - 13)}$$

657 $$\begin{aligned} h &= -\frac{\partial f}{\partial p'_c}\frac{\partial p'_c}{\partial \varepsilon_v^p}\frac{\partial g}{\partial p'} - \frac{\partial f}{\partial r}\left(\frac{\partial r}{\partial \varepsilon_v^p}\frac{\partial g}{\partial p'} + \frac{\partial r}{\partial \varepsilon_s^p}\frac{\partial g}{\partial q}\right) \\ &= \frac{\partial f}{\partial p'_c}\frac{v_0}{\lambda-\kappa}\left(M_g^2 - \eta^2\right) + \frac{\partial f}{\partial r}\frac{v_0}{\lambda-\kappa} s(1-r)\left(\left(M_g^2 - \eta^2\right) + A_d k_g \eta\right) \end{aligned} \quad \text{(A - 14)}$$

$$\frac{\partial f}{\partial p'_c} = \frac{M_f^2}{1-k_f} p'^{\frac{2}{k_f}} \left(2 - \frac{2}{k_f}\right) p_c'^{1-\frac{2}{k_f}} r^{2-\frac{2}{k_f}} \quad \text{(A - 15)}$$

$$\frac{\partial f}{\partial r} = \frac{M_f^2}{1-k_f} p'^{\frac{2}{k_f}} \left(2 - \frac{2}{k_f}\right) r^{1-\frac{2}{k_f}} p_c'^{2-\frac{2}{k_f}} \quad \text{(A - 16)}$$

$$d\boldsymbol{\sigma}' = \mathbf{D}_{\mathbf{ep}} d\boldsymbol{\varepsilon} = \left(\mathbf{D}_{\mathbf{e}} - \frac{\mathbf{D}_{\mathbf{e}} \mathbf{b} \boldsymbol{\alpha}^T \mathbf{D}_{\mathbf{e}}}{\boldsymbol{\alpha}^T \mathbf{D}_{\mathbf{e}} \mathbf{b} + h} \right) d\boldsymbol{\varepsilon} \quad \text{(A - 17)}$$

$$\mathbf{D}_{\mathbf{e}} = \frac{3K}{1+v} \begin{bmatrix} 1\text{-}v & v & v \\ v & 1\text{-}v & v \\ v & v & 1\text{-}v \end{bmatrix} \quad \text{(A - 18)}$$

Appendix B

In the constant soil volume assumption where pore water is regarded as an incompressible fluid, the undrained cylindrical cavity expansion/contraction problem is a simple plane strain deformation problem with five first-order ordinary differential equations for all material points, namely:

$$\frac{D\sigma'_r}{Da_x} = \frac{c_{rr} - c_{r\theta}}{a_x} \tag{B - 1}$$

$$\frac{D\sigma'_\theta}{Da_x} = \frac{c_{\theta r} - c_{\theta\theta}}{a_x} \tag{B - 2}$$

$$\frac{D\sigma'_z}{Da_x} = \frac{c_{zr} - c_{z\theta}}{a_x} \tag{B - 3}$$

$$\frac{Dp'_c}{Da_x} = -\frac{\kappa p'_c}{\lambda - \kappa} \frac{c_{rr} + c_{\theta r} + c_{zr} - c_{r\theta} - c_{\theta\theta} - c_{z\theta}}{a_x\left(\sigma'_r + \sigma'_\theta + \sigma'_z\right)} \tag{B - 4}$$

$$\frac{Dr}{Da_x} = -\frac{\kappa}{\lambda - \kappa} s(1-r)\left(1 + \frac{A_d k_g \eta}{M_g^2 - \eta^2}\right) \frac{c_{rr} + c_{\theta r} + c_{zr} - c_{r\theta} - c_{\theta\theta} - c_{z\theta}}{a_x\left(\sigma'_r + \sigma'_\theta + \sigma'_z\right)} \tag{B - 5}$$

where D/Da_x denotes the material derivative taken along the particle motion path (Lagrangian description), and η denotes the current stress ratio q/p'.

Meanwhile, the constant soil volume assumption would induce a constraint following the equation regarding the current position of any material point a_x and the expanded cavity radius a_0:

$$a_x^2 - a_{x0}^2 = a_0^2 - a_{00}^2 \tag{B - 6}$$

where a_{x0} is the initial position of the material point and a_{00} is the initial cavity radius.

The distribution of pore water pressure $u_w(a_x)$ can be obtained by integrating the radial equilibrium equation:

$$u_w\left(a_x\right) = \sigma'_{r0} + u_{w0} - \sigma'_r\left(a_x\right) - \int_{\infty}^{a_x} \frac{\sigma'_r - \sigma'_\theta}{a_x} da_x \tag{B - 7}$$

Appendix C

In isotropic stress state, the total mean stress change (dp) and lagrangian porosity change ($d\phi$) can be expressed by changes of volumetric strain ($d\varepsilon_v$) and pore water pressure (du_w), as follows:

$$dp = \frac{1}{C_d} d\varepsilon_v + b du_w \tag{C - 1}$$

$$d\phi = -b d\varepsilon_v - \frac{1}{N} du_w \tag{C - 2}$$

with the Maxwell's symmetry condition given by:

$$b = \left(\frac{\partial p}{\partial u_w} \right)_{\varepsilon_v} = -\left(\frac{\partial \phi}{\partial \varepsilon_v} \right)_{u_w} \tag{C - 3}$$

The volumetric compressibility of soil skeleton C_d, the Biot coefficient b appearing in Eq (C - 1) are defined as:

$$\frac{1}{C_d} = \left(\frac{\partial p}{\partial \varepsilon_v} \right)_{u_w}, \quad b = \left(\frac{\partial p}{\partial u_w} \right)_{\varepsilon_v} \tag{C - 4}$$

The Biot coefficient b, Biot modulus N appearing in Eq (C - 2) are defined as:

$$b = -\left(\frac{\partial \phi}{\partial \varepsilon_v} \right)_{u_w}, \quad \frac{1}{N} = -\left(\frac{\partial \phi}{\partial u_w} \right)_{\varepsilon_v} \tag{C - 5}$$

Eqs (C - 4, C - 5) are partial differential equations and the subscripts indicate that the corresponding variables are kept constant.

Considering the relations between the skeleton and mineral solid properties, the compatibility relations can be obtained:

$$b = 1 - \frac{C_s}{C_d}, \quad \frac{1}{N} = (\phi - b) C_s \tag{C - 6}$$

where C_s is the volumetric compressibility coefficient of mineral solid.

In a fully saturated porous medium, the current fluid mass (m_w) per unit volume can be expressed as:

$$m_w = \rho_w \phi \tag{C - 7}$$

Differentiating Eq (C - 7) gives:

$$\frac{dm_w}{\rho_w} = d\phi + \phi \frac{d\rho_w}{\rho_w} \tag{C - 8}$$

The change of fluid density reads as follows:

$$\frac{d\rho_w}{\rho_w} = C_w du_w \tag{C - 9}$$

where C_w is the volumetric compressibility of pore fluid.

From Eqs (C - 1, C - 2, C - 6, C - 8, C - 9), the following equation can be obtained:

$$\frac{dm_w}{\rho_w} = -\left(C_d - C_s\right)dp - \left(\left(\phi C_s - \phi C_w\right) - \left(C_d - C_s\right)\right)du_w \tag{C - 10}$$

In undrained conditions, the mass of the fluid phase is constant and $dm_w = 0$ holds. Thus, the expressions for incremental pore water pressure can be obtained:

$$du_w = \frac{C_d - C_s}{C_d - C_s + \phi\left(C_w - C_s\right)}dp = \frac{d\varepsilon_v - C_s dp}{\phi\left(C_w - C_s\right)} \tag{C - 11}$$

The well-known Skempton coefficient B which indicates the ratio between pore pressure increment and total isotropic stress increment is thus given by:

$$B = \frac{C_d - C_s}{C_d - C_s + \phi\left(C_w - C_s\right)} \tag{C - 12}$$

The compressibility of pore fluid is usually dozens of times that of solid grain. For most clays, the compressibility of solid grains can be neglected ($C_s \approx 0$). With infinitesimal transformation, Eq (C - 11) can be written using Eulerian porosity n and pore fluid's bulk modulus k_w ($k_w = 1/C_w$).

$$du_w = \frac{d\varepsilon_v - C_s dp}{\phi\left(C_w - C_s\right)} \approx \frac{d\varepsilon_v}{nC_w} = \frac{k_w d\varepsilon_v}{n} \tag{C - 13}$$

Data availability statement

The data used to support the findings of this study are available from the corresponding author upon reasonable request.

References

[1] Vesic A S. Expansion of cavities in infinite soil mass[J]. Journal of Soil Mechanics & Foundations Div, 1972, 98(sm3).

[2] Carter J P, Booker J R, Yeung S. Cavity expansion in frictional cohesive soils[J]. Géotechnique, 1986, 36 (3): 349-358.

[3] Yu H S, Houlsby G T. Finite cavity expansion in dilatant soils: loading analysis[J]. Géotechnique, 1991, 41(2): 173-183.

[4] Yu H S. Cavity Expansion Methods in Geomechanics[M]. Dordrecht, the Netherlands: Kluwer Academic Publishers, 2000.

[5] Palmer A C, Mitchell R J. Plane-strain expansion of a cylindrical cavity in clay. Stress-strain behaviour of soils[C]. Proceedings of the Roscoe memorial symposium. Foulis, 1971: 588-599.

[6] Collins I F, Yu H S. Undrained cavity expansions in critical state soils[J]. International journal for numerical and analytical methods in geomechanics, 1996, 20(7): 489-516.

[7] Cao L F, Teh C I, Chang M F. Undrained cavity expansion in modified Cam clay[J]. Géotechnique, 2001, 51(4): 323-34.

[8] Mo P Q, Yu H S. Undrained cavity expansion analysis with a unified state parameter model for clay and sand[J]. Géotechnique, 2017, 67(6): 503-515.

[9] Chen S L, Abousleiman Y N. Exact undrained elasto-plastic solution for cylindrical cavity expansion in modified Cam Clay soil[J]. Géotechnique, 2012, 62(5): 447.

[10] Chen S L, Abousleiman Y N. Exact drained solution for cylindrical cavity expansion in modified Cam Clay soil[J]. Géotechnique, 2013, 63(6): 510.

[11] Chen S L, Abousleiman Y N. Drained and undrained analyses of cylindrical cavity contractions by Bounding Surface plasticity[J]. Canadian Geotechnical Journal, 2016: cgj-2015-0605.

[12] Chen H, Li L, Li J, Wang H. Stress transform method to undrained and drained expansion of a cylindrical cavity in anisotropic modified cam-clay soils[J]. Computers and Geotechnics, 2019, 106: 128-142.

[13] Sivasithamparam N, Castro J. Undrained expansion of a cylindrical cavity in clays with fabric anisotropy: theoretical solution[J]. Acta Geotechnica, 2018, 13(3): 729-746.

[14] Chen S L, Liu K. Undrained cylindrical cavity expansion in anisotropic critical state soils[J]. Géotechnique, 2018, 69(3): 189-202.

[15] Carter J P, Randolph M F, Wroth C P. Stress and pore pressure changes in clay during and after the expansion of a cylindrical cavity[J]. International Journal for Numerical and Analytical Methods in Geomechanics, 1979, 3(4): 305-322.

[16] Hong P Y, Pereira J M, Tang A M, Cui Y J. A two-surface plasticity model for stiff clay[J]. Acta Geotechnica, 2016, 11(4): 871-885.

[17] Avgerinos V, Potts D M, Standing J R. The use of kinematic hardening models for predicting tunnelling-induced ground movements in London clay[J]. Géotechnique, 2015, 66(2): 106-120.

[18] Avgerinos V, Potts D M, Standing J. The use of kinematic hardening models for predicting tunnelling-induced ground movements in London clay[J]. Géotechnique, 2016, 66(2): 106-120.

[19] McDowell GR, Hau KW. A generalised Modified Cam clay model for clay and sand incorporating kinematic hardening and bounding surface plasticity. Granular Matter 2004;6:11-6.

[20] Coussy O. Poromechanics. John Wiley & Sons Inc, 2004.

783 [21] Spang B. Excel add-in for properties of water and steam in SI-units[J]. Water97_v13. xla.
784 Hamburg, 2002.
785 [22] Barnichon J D. Contribution of the bounding surface plasticity to the simulation of gallery
786 excavation in plastic clays[J]. Engineering geology, 2002, 64(2-3): 217-231.
787 [23] Cui Y J, Le T T, Tang A M, et al. Investigating the time-dependent behaviour of Boom clay
788 under thermomechanical loading[J]. Géotechnique, 2009, 59(4): 319-329.
789 [24] Mohajerani M, Delage P, Sulem J, et al. The thermal volume changes of the
790 Callovo-Oxfordian claystone[J]. Rock mechanics and rock engineering, 2014, 47(1): 131-142.
791 [25] Monfared M, Delage P, Sulem J, et al. A new hollow cylinder triaxial cell to study the
792 behavior of geo-materials with low permeability[J]. International Journal of Rock Mechanics and
793 Mining Sciences, 2011, 48(4): 637-649.
794 [26] Van Marcke Ph, Li X L, Bastaens W; Verstricht J et al. The design and installation of the
795 PRACLAY in-situ experiment[R]. Kessel-Lo: Peter De Preter,2013.
796 [27] Charlier R, Chambon R, Collin F, Dizier A, Fauriel S, François B, Fokkens J, Garitte B, Gens
797 A, Gerard P, et al. Timodaz report: Deliverable d13–simulation of lab and in situ tests[R]. 2010.
798 [28] Russell A R, Muir Wood D. A comparison of critical state models for sand under conditions
799 of axial symmetry[J]. Géotechnique, 2010, 60(2): 133-140.
800 [29] Russell A R, Khalili N. On the problem of cavity expansion in unsaturated soils[J].
801 Computational mechanics, 2006, 37(4): 311-330.
802 [30] Borja R I, Lin C H, Montáns F J. Cam-Clay plasticity, Part IV: Implicit integration of
803 anisotropic bounding surface model with nonlinear hyperelasticity and ellipsoidal loading
804 function[J]. Computer Methods in Applied Mechanics and Engineering, 2001, 190(26–
805 27):3293-3323.
806 [31] Rouainia M, Wood D M. A kinematic hardening constitutive model for natural clays with loss
807 of structure[J]. Géotechnique, 2000, 50(2):153-164.
808 [32] Hong P Y, Pereira J M, Cui Y J, et al. An elastoplastic model with combined isotropic–
809 kinematic hardening to predict the cyclic behavior of stiff clays[J]. Computers and Geotechnics,
810 2014, 62(oct.):193-202.
811 [33] McTigue, D. F. Thermoelastic response of fluid‐saturated porous rock[J]. Journal of
812 Geophysical Research Atmospheres, 1986, 91(B9):9533-9542.
813 [34] Mohajerani M, Delage P, Monfared M, et al. Oedometric compression and swelling
814 behaviour of the Callovo-Oxfordia, argillite[J]. International Journal of Rock Mechanics &
815 Mining Sciences, 2011, 48(4):606-615.
816 [35] Barnichon J D. Contribution of the bounding surface plasticity to the simulation of gallery
817 excavation in plastic clays[J]. Engineering Geology, 2002, 64(2-3):217-231.
818 [36] Yang J, Yin Z Y, Liu X F, et al. Numerical analysis for the role of soil properties to the load
819 transfer in clay foundation due to the traffic load of the metro tunnel[J]. Transportation
820 Geotechnics, 2020, 23:100336.
821 [37] Bian X, Hong Z S, Ding J W. Evaluating the effect of soil structure on the ground response
822 during shield tunnelling in Shanghai soft clay[J]. Tunnelling and Underground Space Technology
823 incorporating Trenchless Technology Research, 2016, 58(sep.):120-132.
824 [38] Avgerinos V, Potts D M, Standing J R. The use of kinematic hardening models for predicting
825 tunnelling-induced ground movements in London Clay[J]. Géotechnique, 2016, 66(2):1-15.
826 [39] González N A, Rouainia M, Arroyo M, et al. Analysis of tunnel excavation in London Clay

incorporating soil structure[J]. Géotechnique, 2012, 62(12):1095-1109.
[40] Levasseur S, Y Malécot, Boulon M, et al. Soil parameter identification using a genetic algorithm[J]. International Journal for Numerical & Analytical Methods in Geomechanics, 2010, 32(2):189-213.
[41] Jin Y F, Yin Z Y, Shen S L, et al. A new hybrid real-coded genetic algorithm and its application to parameters identification of soils[J]. Inverse Problems in Science & Engineering, 2016:1-24.
[42] Yin Z Y, Jin Y F, Shen S L, et al. An efficient optimization method for identifying parameters of soft structured clay by an enhanced genetic algorithm and elastic–viscoplastic model[J]. Acta Geotechnica, 2016:1-19.
[43] Jin Y F, Yin Z Y, Shen S L, et al. Investigation into MOGA for identifying parameters of a critical-state-based sand model and parameters correlation by factor analysis[J]. Acta Geotechnica, 2015, 454(5):1-15.
[44] Yin Z Y, Jin Y F, Shen S L, et al. Optimization techniques for identifying soil parameters in geotechnical engineering: Comparative study and enhancement[J]. International Journal for Numerical and Analytical Methods in Geomechanics, 2018, 42(1).
[45] Jin Y F, Yin Z Y, Shen S L, et al. Selection of sand models and identification of parameters using an enhanced genetic algorithm[J]. International Journal for Numerical and Analytical Methods in Geomechanics, 2016, 40(8):1219-1240.

871 **LIST OF TABLES**

874
875
876
877
878
879
880
881
882
883
884
885
886
887
888
889
890
891
892
893
894
895
896
897
898
899
900
901
902
903
904
905
906
907
908
909
910
911

Table 1. The selected parameters of ACC2 model for natural Boom clay

λ	κ	v	$\overline{p}_c'$: MPa	M_f	k_f
0.18	0.02	0.3	6	0.67	0.7
M_g	k_g	r_0	s	A_d	
0.67	0.9	-	8	0.1	

Table 2. Summary of material properties of natural Boom clay

Case	OCR	σ'_r: MPa	σ'_θ: MPa	σ'_z: MPa	k_f	k_g	s	A_d	r_0	$\bar{p}'_c$: MPa	K_0	v_0	s_u: MPa
1	1	2	2	2	0.7	0.9	8	0.1	1	2	1	1.76	0.60
2	1	10	10	10	0.7	0.9	8	0.1	1	10	1	1.47	2.95
3	1	50	50	50	0.7	0.9	8	0.1	1	50	1	1.19	14.29
4	1	5.1	5.1	6	∗	0.9	8	0.1	1	∗	0.85	1.59	1.55
5	1	5.1	5.1	6	0.7	∗	8	0.1	1	5.51	0.85	1.59	1.55
6	2.9	1.91	1.91	2.25	0.7	0.9	∗	0.1	0.34	6	0.85	1.61	1.39
7	2.9	1.91	1.91	2.25	0.7	0.9	8	∗	0.34	6	0.85	1.61	1.39

v_s=1.84, M_g=0.67, '∗' means different values are taken.